Nuclear Instruments and Methods in Physics Research B 374 (2016) 82–89

Contents lists available at ScienceDirect

Nuclear Instruments and Methods in Physics Research B

journal homepage: www.elsevier.com/locate/nimb

On the origin of dislocation loops in irradiated materials: A point of view from silicon

Alain Claverie *, Nikolay Cherkashin

CEMES-CNRS, 29 rue J. Marvig, Toulouse, France

ARTICLE INFO

Article history:
Received 2 September 2015
Accepted 2 September 2015
Available online 29 September 2015

Keywords:
Extended defects
Silicon
Ion irradiation
Nuclear materials
Ostwald ripening

ABSTRACT

Numerous dislocation loops are often observed in irradiated and nuclear materials, affecting many physical properties. The understanding of their origin and of their growth mechanism remains unclear rendering all modeling efforts elusive. In this paper, we remind the knowledge which has been gained during the last 20 years on the formation and growth of extrinsic dislocations loops in irradiated/implanted silicon. From the compilation of a large number of experimental results, a unified picture describing the thermal evolution of interstitial defects, from the di-interstitial stable at room temperature, to "magic-size" clusters then to rod-like defects and finally to large dislocation loops of two types has emerged. All these defects grow by Ostwald ripening, i.e. by interchanging the interstitial atoms they are composed of, and transform from one to the other driven by the resulting reduction of the defect formation energy. A model has been proposed and is now integrated into process simulators which quantitatively describes the thermal evolution of all these defects, based on pertinent formation energies. The influence of the proximity of free surfaces or other recombining interfaces can be integrated, allowing simulating the possible dissolution of defects.

It is suggested that, beyond silicon, the same type of scenario may take place in many materials. Dislocation loops are just one, easily detectable among many, type of defects which forms during the growth of self-interstitials. They do not nucleate but result from the growth and transformation of smaller defects.

1. Introduction

The point defects generated by irradiation in nuclear fuel form extended defects, such as dislocation loops and voids. These extended defects affect the microstructure of the fuel, leading to degradation of its thermal and mechanical properties. Moreover, these defects play an important role in the release of fission gaseous products. In order to fully understand and to be able to accurately predict through modeling the microstructural evolution under irradiation, elucidating the underlying formation mechanisms of these extended defects is important.

There has been much debate in recent years concerning the origin and behavior of the dislocation loops which are observed in uranium dioxide and its surrogates [1]. Two distinct types of extrinsic dislocation loops were observed depending on experimental conditions, both lying on (1 1 1) planes but with different Burgers vector (a/2)⟨1 1 0⟩ or (a/3)⟨1 1 1⟩. Efforts to model their nucleation have faced great difficulties; in particular the formation energies of such dislocation loops appear unrealistically too large when they contain only a few atoms. Moreover, their growth mechanism is still unclear.

Having spent the last 20 years working on the characterization and modeling of extended defects in Silicon, we were told of the above situation by colleagues from the nuclear community and struck by the similarities of this situation with the one the silicon community had to face about twenty years ago. Indeed, the same two types of dislocation loops were found in silicon after "irradiation", actually ion implantation, and it took us a while and lots of experiments to understand then model the formation and thermal evolution of these defects. Today, it is understood and physically based models exist, either analytical or based on Monte Carlo methods, which have been implemented in academic and commercial codes aimed at predicting the effect of processes in semiconductors [2–5].

It is thus the goal of this paper to summarize the main results of the work undertaken by the silicon community to describe the formation and evolution of extrinsic (interstitial) defects in silicon. While these materials, silicon and uranium dioxide, are very

* Corresponding author.
E-mail address: claverie@cemes.fr (A. Claverie).

http://dx.doi.org/10.1016/j.nimb.2015.09.011
0168-583X/

different, we believe that the scenario describing defect evolution in both materials may be quite similar. In particular, we will answer to the following questions, which we have found to summarize the debate animating the nuclear community today:

- Do dislocation loops nucleate from point defects?
- Why are their formation energies unrealistic at small sizes?
- What is the growth mechanism of these loops?
- Why the majority of loops are sometimes observed to be Frank faulted loops and sometimes prismatic (unfaulted) loops?

2. How to form interstitial defects by "irradiation in silicon?

Self-irradiation of course does not exist in silicon. However, there exist different means to generate silicon self-interstitials atoms (Is) which, after annealing, can cluster within extrinsic dislocation loops. Historically, such defects were first observed after high temperature annealing of silicon implanted with dopant atoms. In such cases, the impurity atoms are implanted as interstitials and are activated i.e., locate on substitutional sites, during annealing, ejecting the same number of Si self-interstitials from their original lattice sites. Another simple technique to generate a supersaturation of Is is to directly implant Si^+ ions into silicon, but at sufficiently low doses to prevent the amorphization of the Si crystal to occur [6]. A last technique is to fully amorphize the Si layer by high dose ion implantation with heavy ions such as Ge [7]. In this case, the lattice atoms which are recoiled below the crystalline-amorphous interface accumulate and generate a large supersaturation of Si self-interstitials at this exact location. In these two cases, high temperature annealing leads to the formation of extrinsic dislocations loops.

3. Crystallography of dislocation loops

In general, two types of dislocations are observed (Fig. 1) in different proportions depending on precise experimental conditions. Their characteristics were determined by contrast analysis of TEM images taken under different weak beam conditions and later confirmed by more sophisticated techniques [8,9].

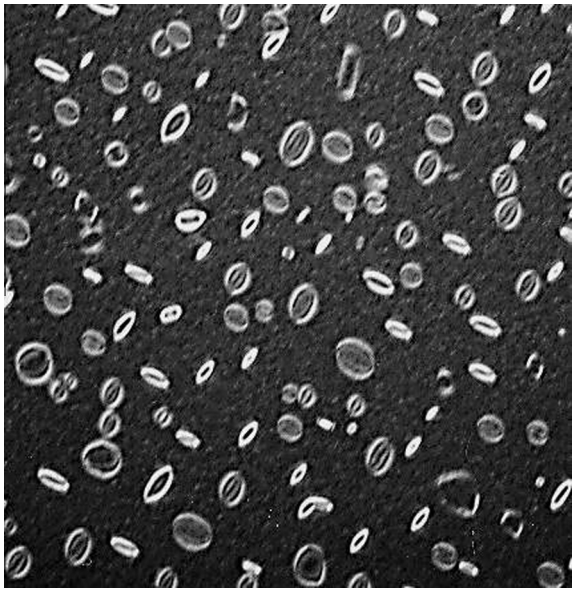

Fig. 1. Typical population of dislocation loops observed by TEM after high temperature annealing (1000 °C, 50 s) of ion implanted silicon (amorphized by Ge, 150 keV, 2×10^{15} ions/cm^2). Two types of dislocations are seen: Frank loops are seen as ellipses, the perfect loops are elongated. Imaging conditions: $\boldsymbol{B} = [001]$, (g, $2g$), $g = 004$.

The {1 1 1} faulted circular Frank loops. These loops are interstitial i.e., they are extrinsic defects. As directly seen in the High Resolution TEM image shown in Fig. 2, they consist of two roughly circular extra {1 1 1} net planes of Si atoms, with a stacking fault displacement vector $\boldsymbol{R} = a/3\langle 1\,1\,1\rangle$ and a planar density of interstitials $d = 15.66\ \mathrm{nm}^{-2}$. The fault is bounded by a Frank partial dislocation whose $\boldsymbol{b} = a/3\langle 1\,1\,1\rangle$, i.e. a pure edge dislocation so that this defect cannot glide and can grow only by climb. There are four variants of such loops, each lying on one of the 4 equivalent {1 1 1} planes.

When plane-viewed in a (0 0 1) Si wafer, with $\boldsymbol{B} = [001]$, they project as ellipses whose large axes (i.e. diameters) are parallel to the two perpendicular [1 1 0] and [1 1 0] directions of the foil. Counting the total number of interstitial Si atoms agglomerated within these loops only requires the measurements of these large axes and of the areal loop density.

The {1 1 1} perfect elongated loops. Perfect $a/2\langle 1\,1\,0\rangle$ loops can appear as elongated, more or less circular, or even hexagonal objects. They have {1 1 1} habit planes and are elongated along the $\langle 1\,1\,0\rangle$ directions perpendicular to their $\boldsymbol{b}$. Each (1 1 1) plane containing three $\langle 1\,1\,0\rangle$ directions, there are twelve variants of such defects. The planar density of Is stored within such defects is thought to be the same than within faulted dislocation loops.

It is striking to note that these two types of dislocation loops are exactly the same than those reported to exist in uranium dioxide and its surrogates.

4. Growth mechanism: Ostwald ripening

Fig. 3 shows the evolution of a population of dislocation loops such as the one shown in Fig. 2 during annealing at 1000 °C. After 50 s of annealing, the population consists of a mixture of both types, faulted and perfect, dislocation loops. When the annealing time increases, only the faulted loops survive. Obviously, the dislocation loops appear larger and in smaller densities as the annealing proceeds.

The statistical analysis of large field of view TEM images, taken under appropriate well-defined conditions and taking into account the contrast rules which apply to each of the 16 (12 + 4) crystallographic variants (10), allows to quantitatively follow the growth of these dislocation loops through the evolution of their size histograms. Fig. 4 shows the result of this analysis for the samples annealed at 1000 °C.

Beside the size increase and density decrease of the loop population, it is important to note that the total number of Si atoms stored within these defects stays constant all along this growth process. For this reason, and from the characteristics of the size histograms, we have deduced that the observed growth was due to the interchange of Si atoms between defects of different sizes following an Ostwald ripening process [10], similarly to what is observed for the growth of precipitates in solid matrices (see Fig. 5).

The Ostwald ripening theory was initially developed to describe the growth of a population of water droplets in equilibrium with a supersaturated vapor. At any given temperature, there exists a dynamical equilibrium between a droplet and the vapor surrounding it. The amplitude of this supersaturation only depends on the diameter of the droplet (formally on its curvature radius). This equilibrium is set by the Gibbs–Thomson equation. This theory can be adapted to the case of solid precipitates in a solid matrix and thus, extended to extrinsic defects in silicon [11,12].

Indeed, dislocations loops are just 2D precipitates of silicon atoms in particular orientation relationships within a silicon

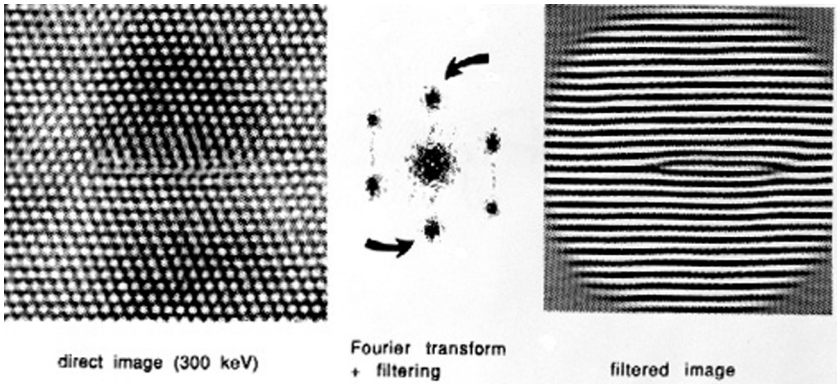

Fig. 2. Left, HREM image of a Frank loop seen edge-on. Fourier filtering of this image (right) clearly evidences the extra (1 1 1) plane which defines the defect.

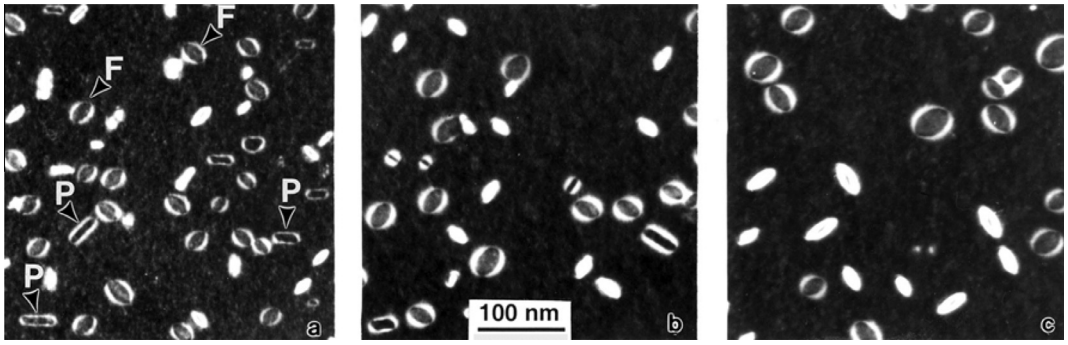

Fig. 3. Thermal evolution of a population of dislocation loops during annealing at 1000 °C. The annealing time increases from 50 s (left) to 200 s (middle) and to 400 s (right).

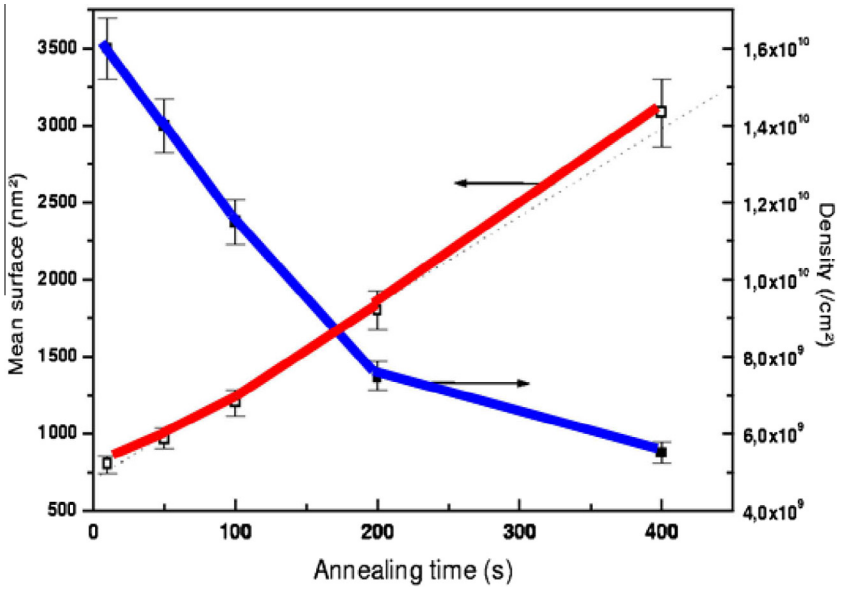

Fig. 4. The evolutions of the mean size ($\langle r \rangle$) and density (d) of a population of dislocation loops during annealing at 1000 °C. Interestingly, the product $\langle r \rangle^2 \cdot d$, proportional to the areal density of Si Is contained within the loops stays constant, evidencing the conservatism of the ripening process.

matrix. Thus, it must be understood that, at the temperature T, every dislocation loop is surrounded by a supersaturation of free Si interstitials C_i/C_i^* (where C_i^* is the equilibrium concentration of Is at T) directly equal to $\exp(E_f/kT)$, where E_f is the formation energy of the defect. This formation energy is the energy cost to add one extra atom to the dislocation loop. It can be analytically calculated from the crystallographic characteristics of the dislocations loops [10,13]. Since the formation energy of a defect monotonously decreases as its size increases, there exist supersaturation gradients between defects of different sizes that make the whole population evolve. A free surface or some interface in the vicinity of these defects will participate to the competition being characterized by its ability to recombine Si self-interstitials.

Moreover, the continuous interchange of Si atoms between defects maintains a mean supersaturation C_i/C_i^* in the region where they are located whose amplitude depends on the formation

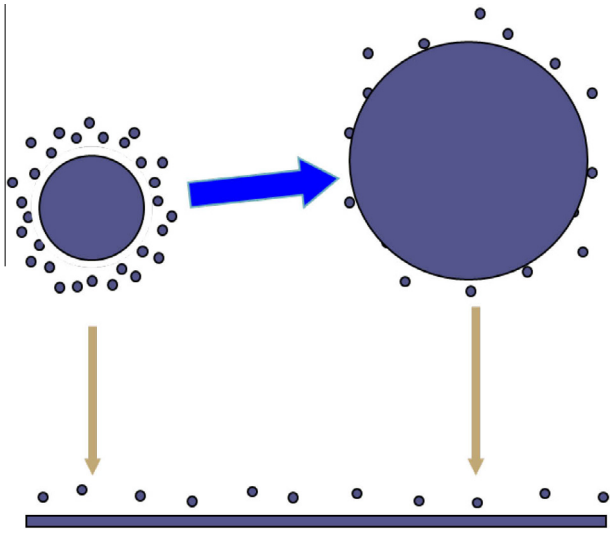

Fig. 5. Concentrations gradient driving the growth of dislocations loops in silicon. The supersaturation and thus, the concentration of Is, surrounding a small loop is larger than that surrounding a large loop, so that Is are transferred from the small to the large loops. However, the surface (bottom) can behave like a defect and capture Is rendering the growth non conservative.

energy of the dislocation loop having the size corresponding to the mean size of the defect population.

For some time, the idea we proposed that the growth of dislocation loops was driven by the diffusion of free Is and not, for example, by the motion and coalescence of the loops, has been somehow controversial. Among many others, a definite proof that the loops were growing following an Ostwald ripening mechanism was provided by the experiment reported in Fig. 6 [14].

For this experiment, several silicon wafers were implanted with increasing ion fluences then identically annealed. As a result, the populations of dislocation loops were found to differ only by the loop densities while their mean sizes were found to be constant and only dependent on the annealing conditions. This invariance of the precipitate size, with respect to the initial concentration of solute atoms (Is), is the signature of a conservative Ostwald ripening. Indeed, as it will be recalled later, the growth rate of a precipitate undergoing Ostwald ripening does not depend on the distance between this precipitate and its neighbors, i.e. on the defect density, but on the difference between its size and the mean size of the population.

Based on these concepts, the growth of dislocation loops could be modeled then simulated for a very large variety of experimental conditions [10,15].

5. Competition between perfect and faulted dislocation loops

As in nuclear materials, the proportions under which the two types of dislocation loops are found strongly depend on the experimental conditions. In some extreme cases, only one type of dislocations loops can even be found. In silicon, the implanted fluence, the annealing temperature but also the annealing ambient, which impacts the ability of the surface to recombine Is, all influence these proportions. The explanation for such a behavior can be understood by calculating the formation energies of both types of loops, as it is shown in Fig. 7. Knowing their respective crystallographic characteristics, the total energies of these dislocation loops can be analytically calculated as a function of their size [13]. From that, the formation energies of these loops can be obtained by simply deriving their total energy with respect

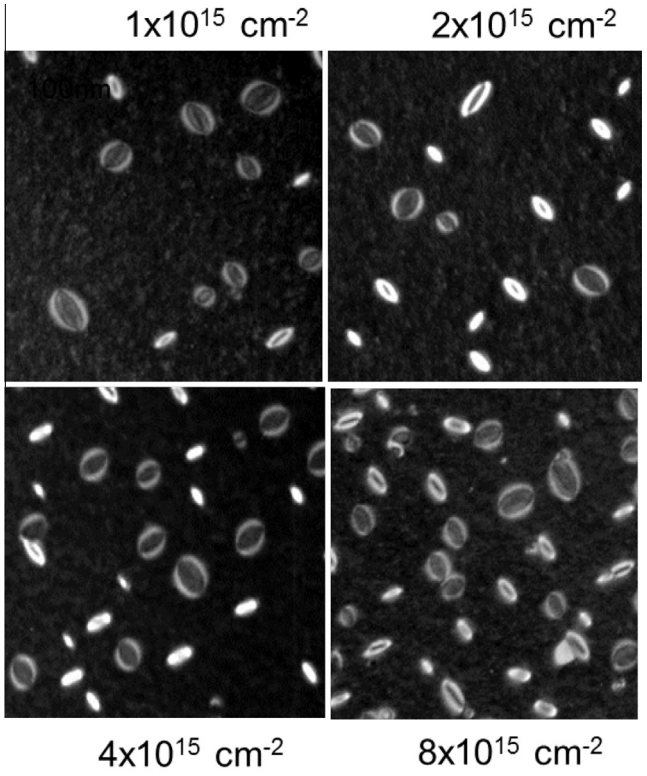

Fig. 6. Loop populations observed after the same 1000 °C, 50 s annealing of silicon implanted with Ge at 150 keV for increasing fluences. Note that the mean size of the loops stays constant. The increasing density of Is available to form the defects only results in a proportional increase of the density of the loop population.

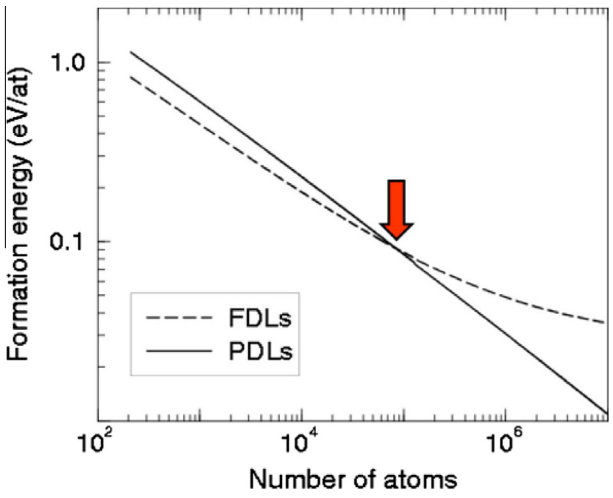

Fig. 7. Comparison of the formation energies of Frank (faulted, FDL) and perfect (PDL) dislocations loops.

to n, the number of Si atoms they contain. The results of such calculations are shown in Fig. 7.

From these calculations, one can see that FDLs are more stable than PDLs at small sizes, but that this reverses when the defects contain more than 90,000 Si atoms, i.e. for radii larger than 40 nm. Indeed, while the formation energy of PDL tends to 0 for infinitely large defects, that of FDL tends to the (1 1 1) stacking fault energy. Thus, the respective proportions under which these loops are found depend on their sizes, as experimentally observed. More discussions on the impact of such differences on the result of the competition can be found in [13].

6. Origin of dislocation loops

Also in silicon, there has been much debate on the origin of dislocation loops. While the Ostwald ripening theory was found to nicely describe the growth of dislocation loops [10,15] of tens of nanometer in diameter, the description of their nucleation was facing serious problems. In particular, the formation energies calculated from the crystallography of the loops were clearly too large at small diameters (because of the elastic energy term), making us doubt that the system would gain reasonably enough energy when precipitating. In other words, it was very improbable that the dislocation loops were directly nucleated from the supersaturation of free Is, the elastic deformation generated by small loops being too large.

Actually, dislocation loops are not the only defects which can be detected by Transmission Electron Microscopy (TEM) techniques when annealing of such ion implanted, Is supersaturated, samples. Depending on the annealing conditions, different types of defects can be observed. Fig. 8 is a pedagogical montage showing the types of defects which form as the annealing temperature is increased.

For low annealing time/temperature combinations, clusters are observed (Fig. 8a). They are too small for their structure to be unambiguously identified by TEM. When annealing for longer times or at a higher temperature, elongated defects, named "Rod Like" (RL) {1 1 3}'s, are observed (Fig. 8b). When annealing further, another type of elongated defects are seen, the RL {1 1 1}'s (Fig. 8c). On this image, one can see the on-going transformation of several of these RL defects into dislocations loops. Thus, dislocation loops result from the transformation of these RL defects. Annealing further, the two types of dislocations loops are observed, and for long enough annealing, only one type is still observed. Actually, the situation is not always that simple and under certain conditions, several types of these defects can be seen to coexist.

It is striking to note that all these defects are of extrinsic character i.e., they consist of extra Si atoms precipitated in the form of clusters, 1 or 2D objects of increasing symmetry and size.

The crystallographic characteristics and thermal behavior of the RL {1 1 3} defects have been studied in details in Ref. [9]. They can be seen as "bundles" of chains of Si di-interstitials lying on {1 1 3} planes and elongated along ⟨1 1 0⟩ directions. They contain about 20 Si atoms per nanometer length. Again, these defects grow by Ostwald ripening, increasing their length and reducing their density, during annealing. Being less stable than the dislocations loops, they are much more sensitive to the proximity of a free surface or interface and depending on conditions, they may dissolve before transforming into RL {1 1 1} defects. This last transformation has been studied by Boninelli et al. [16] and mainly corresponds to a change of the habit plane of a RL defect from a (1 1 3) plane to its neighboring (1 1 1) plane. Once the Si interstitials are aggregated in the form of RL {1 1 1} defects, the symmetries they feel on this habit plane make them wet this plane, transforming into 2D precipitates, i.e. dislocation loops.

7. Origin of RL defects

Immediately following implantation at room temperature, most of the Is in excess to the equilibrium value C_i^* are stored as di-interstitials [17]. After annealing at moderate temperature (600–800 °C), the smallest defects that the TEM can resolve and clearly identify are already 2 nm-long {1 1 3} defects containing at least 40 atoms. Understanding the mechanisms by which these di-interstitials transform into {1 1 3} defects has been an important issue for the silicon community. Using the concept of Ostwald ripening described above, Cowern et al. [18] have built up a model describing the non-conservative Ostwald ripening of clusters of every size from 2 to 500 atoms in presence of a highly recombining surface. Using this model, they have simulated the diffusion of boron delta-doped layers after low dose Si implants and during moderate temperature annealing. The most important finding of their work is that oscillations of the formation energies occur for small, discrete, "magic" sizes.

Clusters of 4, 8 and, to a lesser extent, 12 atoms are superstable (Fig. 9). For larger cluster sizes, the formation energy of these clusters "gently" tends towards 0.8 eV, the value expected for {1 1 3} defects of small sizes. This observation strongly suggest that these magic size clusters are the building blocks for the formation of the RL {1 1 3} defects.

The understanding of the overall thermal evolution and transformation of interstitial defects, from di-interstitials stable at RT to large dislocations loops found after high temperature annealing shows that the concept of "defect nucleation" is not appropriate to describe the formation of dislocation loops or even RL defects. All

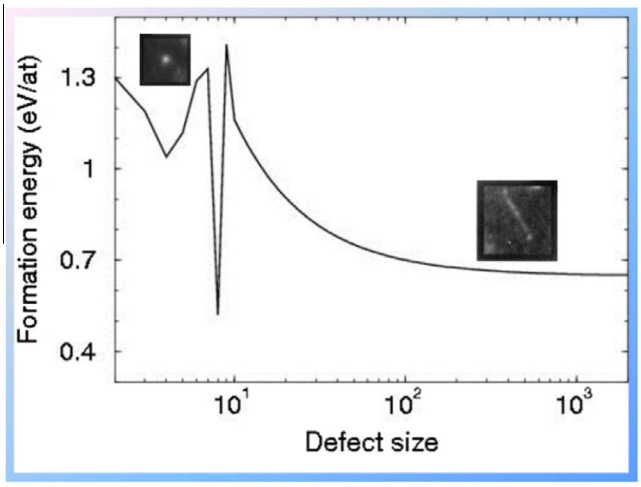

Fig. 9. Formation energies of interstitial clusters as function of the number of atoms they contain. Data extracted from reverse modeling of B diffusion experiments by Cowern et al. [18]. Note the 2 "magic size" superstable clusters of 4 and 8 atoms.

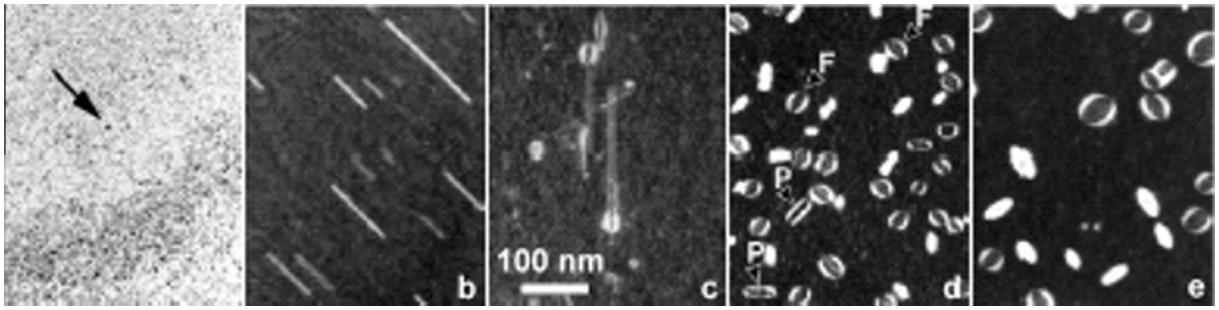

Fig. 8. Types of defects found after annealing of ion implanted silicon. The annealing temperature increases from (a) 500 °C to (e) 1000 °C.

these defects only evolve through diffusion assisted growth and eventually undergo "phase" transformation for certain sizes.

8. Defect energetics

Ostwald ripening has been found to drive both the growth of clusters of small sizes, {1 1 3}s and dislocation loops. In all cases, the driving force for the evolution of a population of defects is the reduction of the formation energy of the defects, i.e., the increase of the binding energy (E_b) of the Si atoms attached to them, as they grow in size and become more stable. In the meantime, and as E_f tends towards 0 the value expected for the perfect crystal, the concentration of Si interstitial atoms in dynamical equilibrium with the defects (Gibbs–Thomson equation) decreases back to its equilibrium value, C_i^*.

From an energetic point of view, the thermal evolution of all types of interstitial defects reflects the defect hierarchy in terms of formation energy, as shown in Fig. 10.

From the di-interstitials, small clusters grow through magic sizes until forming RL {1 1 3} defects of small sizes. Once these {1 1 3}s are formed, they grow in size and reduce their density, again as a result of ripening. Their total energy can be analytically calculated from their crystallographic characteristics i.e., by taking into account the two edge dislocations plus the two mixed dislocations plus the stacking fault energy which altogether define them [19]. This formation energy curve gently tends towards its asymptotical limit at 0.6 eV, as shown in Fig. 10.

When incorporating in this graph the formation energies of the two types of dislocations loops shown in Fig. 7, we note the crossing of these formation energies with that associated to the RL{1 1 3} defects. This shows that it energetically more favorable for the supersaturated crystal to form a long RL{1 1 3} containing up to five hundreds of Si atoms than to "nucleate" a dislocation loop of 5 nm radius, whatever its type. This is confirmed experimentally, as dislocation loops smaller than that size have never been observed. When growing, the largest RL{1 1 3} defects will transform into RL{1 1 1}s themselves wetting the (1 1 1) planes and becoming loops. The probability to form one or the other type of loop depends on the formation energy difference between them which in turn depends on the number of Si interstitials they contain. This also nicely explains experimental observations [13].

All the intriguing characteristics of the concomitant thermal behavior of all these defects, can be understood from this figure. For example, a PDL of 1000 atoms can be more stable than a RL {1 1 3} but less stable than a FDL, all containing the same number of atoms.

The Ostwald ripening of such defects maintains in the region a supersaturation of Is which decreases as the formation energy of the extended defects decreases. For this reason, we have plotted on the right vertical axis of Fig. 10 the supersaturation of Is in dynamical equilibrium with these defects for a temperature of 800 °C. This curve also shows a hierarchy of levels of non-equilibrium diffusion, ranging from supersaturations C_i/C_i^* of 10^6 in the presence of small clusters through 10^3 in the presence of {1 1 3}s, to C_i/C_i^* in the range 100 down to 1 as the loops evolve and grow in size.

While this curve determines the amount of supersaturation in the region of the sample where the defects stand, its spatial extension towards the free surface of a real material (a wafer for Si) or towards some interface depends on the characteristics of that surface or interface. A highly recombining surface will compete with the defects during Ostwald ripening if situated close enough to the defects. Fig. 11 shows the situation.

From the defect region, the supersaturation $S = C_i/C_i^*$ in equilibrium with the defect population linearly decreases to reach 0 at the fictitious distance L (recombination length) from the surface [20]. This necessary pinning of the supersaturation at the surface creates a concentration gradient and thus a flux of Is leaving the defect region. The ripening is no longer conservative and, for example, dissolution of the RL{1 1 3} defects can occur before their transformation into loops. More generally, the extent to which the defects evolve before finally evaporating to the surface or some recombining interface, depends on the total number of available Is, on the efficiency of that surface (interface) to incorporate Si interstitials (recombination length or time) and on the distance between the "defect" layer and the surface (interface).

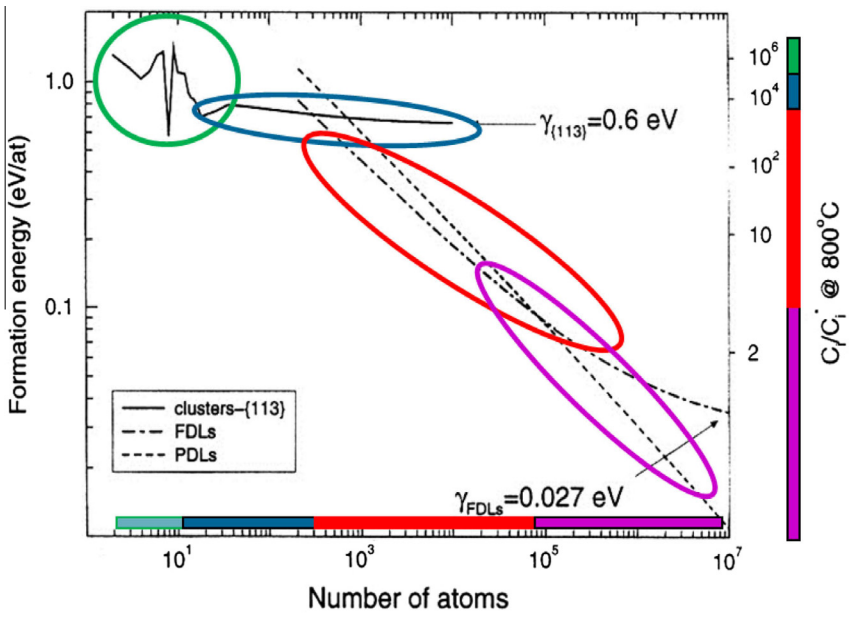

Fig. 10. Formation energy (left axis) of the different types of extrinsic defects as a function of their size and corresponding values of the Si(int)s supersaturation in dynamical equilibrium with them, at 800 °C (right axis). Clusters in green, RL defects in blue, DL in red and purple. (For interpretation of the references to color in this figure legend, the reader is referred to the web version of this article.)

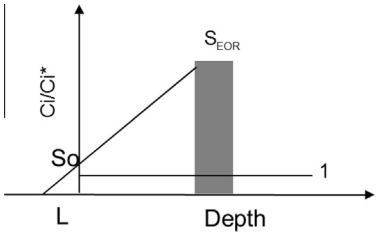

Fig. 11. Variation of the amplitude of the Si(int) supersaturation generated by a defect-rich region (gray) located close to a recombining surface or interface.

9. Modeling of defect growth

Today, different simulation codes exist which describe the growth and evolution of these defects in silicon. They have evolved upon time, from time consuming analytical to more efficient moment based, and even to atomistic kinetic Monte Carlo versions, each having its pros and cons. However, they all rely on the Physics we initially proposed, based on our experimental observations, and which is recalled below.

We describe the growth of "precipitates" in a matrix by calculating the difference between the capture (F_n) and emission (R_n) rates of every cluster of size n. The growth rate is classically writtenas the product of the capture area of the particle by the net flux of atoms towards it. In the case of a diffusion-limited growth, this growth rate can be written [21],

$$\frac{dn}{dt} = |F_n - R_n| = D_i C_i^* A_n \left.\frac{dS}{dR}\right|_{R=r} = D_i C_i^* \frac{A_n}{R_{eff}} (\bar{S} - S(n)), \quad (1)$$

where $D_i C_i^*$ is the self-diffusivity of the impurity atoms within the host matrix. A_n is the capture area of the precipitate. Because R_{eff} represents the radial extension of the diffusion field, A_n/R_{eff} is characteristics of the capture efficiency of the defect. S is the mean supersaturation of these Si interstitials within the matrix and $S(n)$ the supersaturation of interstitials in equilibrium with a precipitate containing n atoms. $S(n)$ is given by the Gibbs–Thomson equation and can be written,

$$S(n) = \exp\left[\frac{E_f(n)}{kT}\right], \quad (2)$$

$E_f(n)$ being the formation energy of a precipitate containing n atoms. The emission rate (R_n) is thus proportional to the formation energy of the particle and is given by,

$$R_n = D_i C_i^* \times \frac{A_n}{R_{eff}} \times \exp\left[\frac{E_f(n)}{kT}\right]. \quad (3)$$

The capture rate (F_n) is a function of the environment of the precipitate and is proportional to S, the mean supersaturation of Si interstitials between the precipitates,

$$F_n = D_i C_i^* \times \frac{A_n}{R_{eff}} \times \bar{S}. \quad (4)$$

Both the capture efficiency (A_n/R_{eff}) and the formation energy (E_f) depend on the geometry of the defect. The model is based on a set of $(n+1)$ coupled differential equations. The first n equations describe the flux of atoms from particles of size n to particles of size $n+1$ and $n-1$,

$$\frac{dN_n}{dt} = F_{n-1}N_{n-1} - F_n N_n + R_{n+1}N_{n+1} - R_n N_n. \quad (5)$$

This equation drives the growth of the defects both in terms of sizes and densities. The last equation describes the "free component" of the Si atoms i.e., the concomitant evolution of the free Si interstitials supersaturation in dynamical equilibrium with the extended defects,

$$\bar{S} = \frac{\sum_{n=2}^{\infty} \beta_n R_n N_n}{D_i C_i^* \left(\left(\sum_{n=2}^{\infty} \beta_n R_n N_n \frac{A_n}{R_{eff}} N_n \right) + \frac{1}{L_{surf} + r_p} \right)}. \quad (6)$$

N_n is the number of precipitates of size n. L_{surf} is the recombination length at the surface and r_p the depth position of the defects. The quantity β is the number of Si atoms released by the break-up of a cluster ($\beta = 2$ for $n = 2$, $\beta = 1$ otherwise). This last equation describes the time evolution of the supersaturation mean-field centered on the defects.

Exploring and discussing the result of this model and of those based on the same physics would take us far beyond the scope of this paper. It is important to note that they all rely on the formation energies shown in Fig. 10 which provides the driving force for the growth of the defects. A special attention must be paid to the description and calculation of the capture areas associated to all these defects as they heavily depend on the defect geometries and associated strain fields which surround them. However, all these models are now accurate, having been tested and eventually calibrated against hundreds of experimental results about defect growth and dopant diffusion. They are indeed absolutely needed to simulate the diffusion of dopants during silicon processing for the fabrication of transistors.

10. Conclusions

Dislocations loops are observed in silicon, after ion implantation and high temperature annealing. They arise from the precipitation of Si interstitials atoms in excess in the lattice. Interestingly, they are of the two same types than observed in uranium oxide and its surrogates. These dislocation loops do not nucleate from a supersaturation of free Si self-interstitials but originate from the transformation of RL defects which themselves originate from the growth of interstitial clusters during annealing. All these interstitial defects grow by Ostwald ripening, i.e. by interchanging the Si atoms they are composed of, in such a way that more stable defects grow at the expense of less stable defects. The driving force for such an evolution is provided by the reduction of the formation energy of the defects as they grow in size or change their crystallographic characteristics. Finally, we have shown how a physically based model can be set up to describe such an evolution.

We hope that this summary of the main results obtained by the silicon community will be of some pertinence and helpful to the nuclear community, as it is very probable that the same type of behavior is at the origin of the observation of dislocations loops in self-irradiated uranium oxides and its surrogates.

References

[1] Y. Miao et al., J. Nucl. Mater. 445 (2014) 209–217.
[2] C. Ortiz, P. Pichler, T. Fuhner, F. Cristiano, B. Colombeau, N.E.B. Cowern, A. Claverie, J. Appl. Phys. 96 (N9) (2004) 4866–4877.
[3] I. Martin-Bragado, I. Avci, N. Zographos, M. Jaraiz, P. Castrillo, Solid State Electron. V52 (9) (2008) 1430–1436.
[4] K.R.C. Mok, B. Colombeau, F. Benistant, R.S. Teo, S.H. Yeong, B. Yang, M. Jaraiz, F. S. Chu, IEEE Trans. Electron Devices 54 (9-54) (2007) 2155–2163, http://dx.doi.org/10.1109/TED.2007.
[5] E.M. Bazizi, A. Pakfar, P.F. Fazzini, F. Cristiano, C. Tavernier, A. Claverie, N. Zographos, C. Zechner, E. Scheid, Thin Solid Films 518 (9) (2010) 2427–2430, http://dx.doi.org/10.1016/j.tsf.2009.
[6] A. Claverie, C. Bonafos, D. Alquier, A. Martinez, Solid State Phys. V47–48 (1996) 195.
[7] A. Claverie, L.F. Giles, M. Omri, B. De Mauduit, G. Ben Assayag, D. Mathiot, Nucl. Instr. Meth. Phys. Res. B 147 (1999) 1.
[8] B. De Mauduit, L. Laânab, C. Bergaud, M.M. Faye, A. Martinez, A. Claverie, Nucl. Instr. Meth. Phys. Res. B 84 (1994) 190.
[9] A. Claverie, N. Cherkashin, in: A. Claverie (Ed.), Transmission Electron Microscopy for Micro/nano electronics, ISTE Wiley, 2012. Chapter 10.
[10] C. Bonafos, D. Mathiot, A. Claverie, J. Appl. Phys. 83 (6) (1998) 3008–3017.
[11] A. Claverie, B. Colombeau, G. Ben Assayag, C. Bonafos, F. Cristiano, M. Omri, B. De Mauduit, Mater. Sci. Semin. Proc. 3 (2000) 269.
[12] A. Claverie et al., Appl. Phys. A 76 (2003) 1025–1033.

[13] F. Cristiano, J. Grisolia, B. Colombeau, M. Omri, B. De Mauduit, F. Giles, N.E.B. Cowern, A. Claverie, J. Appl. Phys. 87 (12) (2000) 8420–8428.
[14] B. Colombeau, G. Ben Assayag, A. Claverie, C. Armand, F. Olivie, F. Cristiano, Nucl. Instr. Meth. B 186 (2002) 276–280.
[15] E. Lampin, V. Senez, A. Claverie, J. Appl. Phys. V85 (12) (1999) 8137–8144.
[16] S. Boninelli, N. Cherkashin, F. Cristiano, A. Claverie, Appl. Phys. Let. 89 (2006) 161904.
[17] J.W. Corbett, J.P. Karins, T.Y. Tan, Nucl. Instr. Meth. Phys. Res. B 457 (1981) 182–183.
[18] N.E.B. Cowern, G. Mannino, P.A. Stolk, A. Claverie, Phys. Rev. Lett. 82 (22) (1999) 4460–4463.
[19] B. Colombeau, F. Cristiano, A. Altibelli, C. Bonafos, G. Ben Assayag, A. Claverie, Appl. Phys. Lett. 78 (2001) 940–942.
[20] N.E.B. Cowern, D. Alquier, M. Omri, A. Claverie, A. Nejim, Nucl. Instr. Meth. Phys. Res. B 148 (1999) 257.
[21] A.H. Gencer, S.T. Dunham, J. Appl. Phys. 81 (1997) 631.